Proton-Prompted Ligand Exchange to Achieve High-Efficiency CsPbI$_3$ Quantum Dot Light-Emitting Diodes

Yanming Li[1,2], Ming Deng[1,2,4], Xuanyu Zhang[1,2,5], Lei Qian[1,2,3], Chaoyu Xiang[1,2,3] ✉

HIGHLIGHTS

- A new proton-promoted in situ ligand exchange strategy based on CsPbI$_3$ quantum dots.

- The ligand exchange strategy maintains the quantum confinement effect of quantum dots and significantly improves the stability and photophysical properties of CsPbI$_3$ quantum dots.

- The performance of light-emitting diodes based on CsPbI$_3$ quantum dots is significantly improved, the external quantum efficiency is increased from 18.63% to 24.45%, and the half-operational lifetime is increased by 70 times.

ABSTRACT CsPbI$_3$ perovskite quantum dots (QDs) are ideal materials for the next generation of red light-emitting diodes. However, the low phase stability of CsPbI$_3$ QDs and long-chain insulating capping ligands hinder the improvement of device performance. Traditional in-situ ligand replacement and ligand exchange after synthesis were often difficult to control. Here, we proposed a new ligand exchange strategy using a proton-prompted in-situ exchange of short 5-aminopentanoic acid ligands with long-chain oleic acid and oleylamine ligands to obtain stable small-size CsPbI$_3$ QDs. This exchange strategy maintained the size and morphology of CsPbI$_3$ QDs and improved the optical properties and the conductivity of CsPbI$_3$ QDs films. As a result, high-efficiency red QD-based light-emitting diodes with an emission wavelength of 645 nm demonstrated a record maximum external quantum efficiency of 24.45% and an operational half-life of 10.79 h.

Yanming Li, Ming Deng, and Xuanyu Zhang are contributed equally to this work.

✉ Chaoyu Xiang, xiangchaoyu@nimte.ac.cn

1   Laboratory of Advanced Nano-Optoelectronic Materials and Devices, Qianwan Institute of CNITECH, Ningbo 315300, People's Republic of China
2   Division of Functional Materials and Nanodevices, Ningbo Institute of Materials Technology and Engineering, Chinese Academy of Sciences, Ningbo 315201, People's Republic of China
3   Zhejiang Provincial Engineering Research Center of Energy Optoelectronic Materials and Devices, Ningbo Institute of Materials Technology & Engineering, Chinese Academy of Sciences, Ningbo 315201, People's Republic of China
4   Faculty of Electrical Engineering and Computer Science, Ningbo University, Ningbo 315211, Zhejiang, People's Republic of China
5   University of Nottingham Ningbo China, Ningbo 315100, People's Republic of China

1 Introduction

Metal halide perovskite nanocrystals (NCs) are considered the next-generation materials of light-emitting diodes (LEDs) due to their high fluorescence quantum yield (PLQY), continuously adjustable band gap, high color purity, and solution processing [1–5]. $CsPbI_3$ perovskite NCs with excellent thermal stability and ideal band gap (-1.7 eV) are widely used in red light-emitting diodes and solar cells (SCs) [6–8]. The size control of small $CsPbI_3$ quantum dots (QDs) by quantum confinement effect makes it possible to meet the red standard for wide color gamut high-definition Rec. 2020 displays [9–11]. However, the high specific surface area of the small-size $CsPbI_3$ QDs brings a high density of non-radiative recombination defects [12]. Traditionally, it is difficult for long-chain organic ligands, such as oleylamine (OA) and oleylamine (OAm), to sufficiently passivate the defects on the surface of small QDs due to the large steric hindrance. In addition, the fatty long-chain also hinders the charge transfer between QDs [13, 14]. Thus, replacing the long-chain ligands with short ligands is the key to improving the performance of LEDs devices based on small-size $CsPbI_3$ QDs.

In-situ ligand replacement and ligand exchange after synthesis were two common methods to replace the long-chain insulating ligands [15–17]. However, balancing the colloid stability and short ligand passivation is a challenge while maintaining the $CsPbI_3$ QDs confinement. During the synthesis reaction, the length of the fatty chain and the binding energy of the functional group of the ligands strongly affected the shape and size of QDs [18–20]. Besides, the low boiling point of short-chain ligands was hard to use in high-temperature thermal injection reactions. The ligand exchange after QDs synthesis requires polar solvents to remove the original long-chain ligands [21]. However, the high-ionic structure and low phase stability of perovskite QDs limit the selection of ligand solvents that can be used [22, 23]. Strong polar solvents, such as methanol, will damage the structural stability of perovskite nanocrystals. The loss of ligands during the post-treatment leads to agglomeration or even decomposition of $CsPbI_3$ QDs [24, 25]. Therefore effective ligand exchange strategy is an important way to improve the stability and charge transfer performance of perovskite QDs, especially for small-size $CsPbI_3$ QDs.

Here, we reported a new strategy of proton-prompted short-chain ligand exchange in the reaction cooling stage of perovskite QDs synthesis. Hydroiodic acid (HI) provided protons and dissolved a short-chain ligand 5-aminopentanoic acid (5AVA), which traditionally can only dissolve in strongly polar solvents. The introduction of protons triggered the desorption of long-chain oleylamine (OA) and oleylamine (OAm) ligands on the surface of QDs. At the same time, the amine functional groups of 5AVA ligands were protonated, which promoted their binding to the QDs surface. Meanwhile, iodine ions provided an iodine-rich environment and maintained the size of $CsPbI_3$ QDs. Through this strategy, we synthesized stable small-size $CsPbI_3$ QDs, and the ligand exchange did not affect the crystal structure and shape of QDs. Short-chain 5AVA ligands with bifunctional groups improved the optical properties of $CsPbI_3$ QDs as well as the conductivity of the QD films. Based on the $CsPbI_3$ QDs with 5AVA ligands, high-efficiency red QD-based light-emitting diodes (QLEDs) with a peak quantum efficiency (EQE) of 24.45% and stable electroluminescence at 645 nm emission wavelength were achieved. Compared with the control device, the brightness of the device was significantly improved to 7494 cd m^{-2}. And the half-operational lifetime was improved to 10.79 h, which was 70 times higher than the control device.

2 Experimental Section

2.1 Materials

Lead iodide (PbI_2, Macklin, 99.999%), zinc iodide (ZnI_2, Aladdin, 99.99%), cesium carbonate (Cs_2CO_3, Sigma-Aldrich), 5-aminovaleric acid (5AVA, Aladdin, 97%), hydroiodic acid (HI, Aladdin, 55.0%–58.0%), octadecene (ODE, Sigma-Aldrich, 90%), oleic acid (OA, Sigma-Aldrich, 90%), oleylamine (OAm, Aladdin, 90%), n-hexane (Aladdin, 98%), n-octane (Aladdin, 99%), methyl acetate (Sinopharm Chemical Reagent Co., Ltd. (SCRC), 98%), ethyl acetate (Aladdin, 99.9%), poly(3,4-ethylenedioxythiophene) polystyrene sulfonate (PEDOT:PSS, 4083, Xi'an Polymer Light Technology Corp.), poly[bis(4-phenyl)(2,4,6-trimethylphenyl)amine](PTAA, Lingzhi Technology Co., Ltd.), 2,4,6-tris[3-(diphenylphosphinyl)

phenyl]-1,3,5-triazine (PO-T2T, Xi'an Polymer Light Technology Corp.), 3,3′-[5′-[3-(3-pyridinyl)phenyl][1,1′:3′,1″-terphenyl]-3,3″-diyl]bispyridine (TmPyPB, Xi'an Polymer Light Technology Corp.), lithium fluoride (LiF, Xi'an Polymer Light Technology Corp., 99.9%), which were directly used.

2.2 Synthesis of CsPbI$_3$ QDs

2.2.1 Preparation of 5AVAI Ligand Solution

The 5AVA of (0.1, 0.2, 0.3) mmol (M) was dissolved in 1.5 times HI, and then 1 mL ethyl acetate was added to prepare the 5AVAI solution. The 5AVAI solution was heated to 80 °C for subsequent ligand treatment.

2.2.2 Preparation of Cs-OA Solution

144 mg of Cs$_2$CO$_3$, 11 mL of ODE, and 6 mL of OA were loaded into a 50 mL 3-neck flask. The mixture is dried for 15 min at room temperature in a vacuum. Then, the mixture was heated to 100 °C until a transparent solution was formed and heated at 100 °C for 30 min under argon flow. The obtained Cs-OA solution was stored in an argon atmosphere and preheated to 100 °C for subsequent perovskite QD synthesis.

2.2.3 Synthesis and Purification of CsPbI$_3$ QDs Treated with 5AVAI

170 mg PbI$_2$, 345 mg ZnI$_2$, and 6 mL ODE were loaded into a 50 mL three-necked flask and dried under argon flow at 120 °C for 1 h. Then, 1 mL OA and 2 mL OAm were injected at 120 °C under argon flow. The temperature was increased to 150 °C and Cs-oleate (2.2 mL of the stock solution prepared as described above) was swiftly injected. After five seconds, the reaction mixture was immediately cooled to 100 °C by immersing in a cold water bath, the prepared 5AVAI ligand solution was swiftly injected, and then the reaction mixture was cooled down to room temperature.

The crude solution was centrifuged at 5000 rpm for 1 min to remove unreacted precursor precipitate and then transferred to two 50 mL centrifuge tubes equally. Anti-solvent ethyl acetate and methyl acetate were added to the obtained crude solution (the volume ratio of QDs solution, ethyl acetate, and methyl acetate was 1:1:3), and then centrifuged at 7000 rpm for 2 min. The obtained precipitate containing CsPbI$_3$ QDs was re-dispersed in 1 mL of hexane and centrifuged at 5000 rpm for 1 min to remove non-perovskite precipitates. The preliminary purified QDs solution of 1 mL was added to 6 mL methyl acetate and 6 mL ethyl acetate to precipitate again and centrifuged at 4000 rpm for 5 min. The obtained CsPbI$_3$ QDs were redispersed in 1 mL of octane and centrifuged at 5000 rpm for 1 min. Finally, the QDs solution was filtered by a 0.22 μm poly(tetrafluoroethylene) filter.

2.2.4 Synthesis and Purification of CsPbI$_3$ QDs without 5AVAI Treatment

170 mg PbI$_2$, 345 mg ZnI$_2$, and 6 mL ODE were loaded into a 50 mL three-necked flask and dried under argon flow at 120 °C for 1 h. Then, 1 mL OA and 2 mL OAm were injected at 120 °C under argon flow. The temperature was increased to 150 °C and Cs-oleate (2.2 mL of the stock solution prepared as described above) was swiftly injected. After five seconds, the reaction mixture was immediately cooled down to room temperature by immersing it in a cold-water bath.

The subsequent purification process is the same as the purification of CsPbI$_3$ QDs treated by 5AVAI.

These synthesized QDs samples are stored for further characterization and fabrication of LEDs devices.

2.3 Fabrication and Characterization of CsPbI$_3$ QDs-Based LEDs

The ITO-coated glass substrates were ultrasonicated with ITO cleaning solution, deionized water, acetone, isopropanol, and ethanol for 30 min respectively. Then, these substrates were put into an ultraviolet-ozone cleaner for 15 min. PEDOT:PSS solution was spin-coated on ITO-coated glass substrates at 4500 rpm for 45 s and annealed at 150 °C for 20 min in air. The coated substrate was moved into a nitrogen glove box. PTAA solution (8 mg mL^{-1}) in chlorobenzenes was spin-coated on the PEDOT:PSS layer at 2000 rpm for 45 s and annealed in a nitrogen atmosphere at 120 °C for 20 min. The CsPbI$_3$ QDs or 5AVAI-CsPbI$_3$ QDs in octane (10 mg mL^{-1}) were spin-coated onto the PTAA layer by the spin-coater at 4000 rpm for 45 s and

annealed at 60 °C for 5 min. Finally, under the condition of high vacuum (-2×10^{-4} Pa), a 6 nm TmPyPB layer, 40 nm PO-T2T layer, 1 nm LiF layer, and 100 nm Al electrode were deposited by thermal evaporation system. The device's active area was 4 mm^2. Subsequently, the performance of the fabricated LED device is tested. The EL spectrum was collected by Ocean Optics USB 2000 + spectrometer, and the *J-L-V* characteristic of the device was measured by Keithley 2400 source table. The life of LEDs devices was measured by using a life test system (Guangzhou Jinghe Equipment Co., Ltd.) under ambient conditions.

2.4 Characterizations

The ultraviolet–visible (UV–vis) absorption spectrum of the QD solution was obtained by the PerkinElmer instrument. Photoluminescence (PL) spectrum of QD solution was measured on HORIBA fluorescence spectrometer (FL3-111) and excited at 365 nm. PLQY of QD solution was measured by Otsuka QE2100 device, diluted with hexane in quartz cuvette, and excited at 365 nm. Transmission electron microscope (TEM) images were obtained by Talos F200X instrument, and the accelerating voltage was 200 kV. Atomic force microscope (AFM) images of QD thin films were collected in tapping mode with a Dimension ICON instrument. Powder X-ray diffraction (XRD) patterns were recorded using a D8 ADVANCE diffractometer with Cu Kα radiation ($\lambda = 1.54178$ Å). Fourier transform infrared (FTIR) spectrum of QDs powder was obtained by Fourier infrared spectrometer (IS50). The time-resolved photoluminescence luminescence decay spectra of QDs were obtained by FL3-111 spectrometer.

3 Results and Discussion

3.1 Proton-Prompted Ligand Exchange

CsPbI$_3$ QDs with or without 5AVA were synthesized by a modified thermal injection method (see the experimental part for details). 5AVA ligands were dissolved in excess HI solution to form 5-Ammonium valeric acid iodide (5AVAI) as the precursor (Fig. S1a). Bright CsPbI$_3$ QDs were synthesized by injection 5AVAI at the cooling stage after the nucleation of CsPbI$_3$ QDs (Fig. S1b). There is a highly dynamic binding between the surface-capped ligands of perovskite

QDs [26]. For the traditional OA and OAm capped QDs, there is a balance between the ionization form and molecular form of these ligands (OA$^-$ + OAmH$^+$ ⇌ OAH + OAm or OAmH$^+$ + I$^-$ ⇌ OAm + HI) [27, 28]. This dynamic binding reaction leads to the desorption of ligands during the separation and purification of QDs, resulting in a decrease in the stability and optical properties of QDs. In the proton-prompted strategy, the protons provided by excess HI drive the dynamic equilibrium transfer of OA$^-$ and OAmH$^+$ ligands bound to QDs surface to molecular form. Then 5AVAI ligands with bifunctional groups bind to surface sites left by OA and OAm ligands. The CsPbI$_3$ QDs synthesized by HI treatment (without 5AVA) almost decomposes (Fig. S1c), which is attributed to the proton provided by HI which promotes the shedding of OA and OAm ligands on the surface of QDs. In addition, the I$^-$ from HI can fill the I$^-$ vacancy defects on the surface of QDs. Figure 1a illustrates the strategy of in situ exchange of the HI-driven 5AVA ligands with the OA/OAm ligands.

The optical properties of CsPbI$_3$ QDs were characterized to study the influence of 5AVAI ligands. As the amount of 5AVAI increased, the first exciton absorption peak and PL peak shifted to a shorter wavelength, as shown in Fig. 1b. The blue shift of the absorption peak and PL peak is attributed to the decrease in QDs size due to the increase of iodine ions in the reaction system [29]. The photos of CsPbI$_3$ QDs synthesized with different 5AVAI amounts under ultraviolet light (365 nm) are shown in Fig. 1c. With the increase of the 5AVAI amount, the PLQY of QDs increased, reaching the maximum value of 95% at 0.2 M (Fig. 1d). These results show that the introduction of 5AVAI in the synthesis process can reduce the size of CsPbI$_3$ QDs, effectively passivate the surface defects of CsPbI$_3$ QDs, and improve the optical properties of QDs. However, for the synthesized CsPbI$_3$ QDs, the CsPbI$_3$ QDs are decomposed after introducing 5AVAI ligands for ligand exchange (Fig. S2), which is attributed to the strong polarity of HI leading to the shedding of ligands on the surface of the QDs.

The optical properties and morphology of CsPbI$_3$ QDs synthesized with 0.2 M 5AVAI and without 5AVAI were compared. With the same synthesis condition, the PL peak wavelength with 5AVAI is shorter than that of PL without 5AVAI treatment. The full width at half maximum (FWHM) is narrower (38 and 42 nm for with 5AVAI and without 5AVAI, respectively), which indicates that QDs treated by 5AVAI has smaller size and more uniform size distribution.
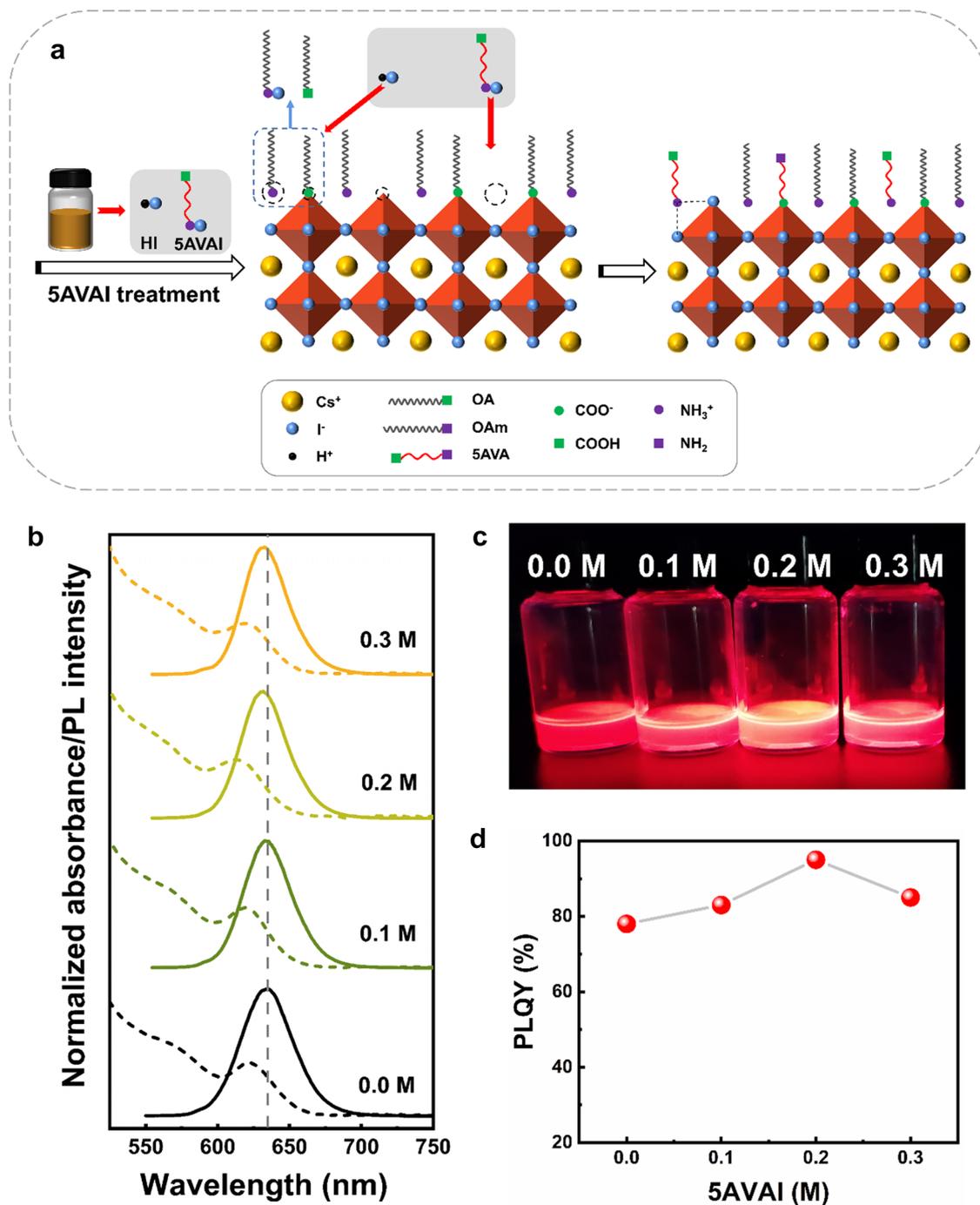
Fig. 1 **a** Strategy diagram of in situ exchange between 5AVA ligand and OA/OAm ligand driven by HI. **b** The UV–vis absorption and fluorescence spectra of CsPbI$_3$ QDs purified once with different 5AVAI content. **c** Photos of CsPbI$_3$ QDs treated with different 5AVAI amounts under ultraviolet light (365 nm). **d** PLQY of CsPbI$_3$ QDs treated with different amounts of 5AVAI

Iodine-rich environment inhibits the growth and size distribution broadening of QDs caused by Ostwald ripening. The PLQY of QDs with 5AVAI is 87%, while the PLQY of QDs without 5AVAI treatment is 69%, indicating that

5AVAI effectively passivates the surface defects of QDs. Furthermore, we studied the stability of QDs under ambient conditions (Fig. 2b). The QDs treated by 5AVAI were still more than 70% after 20 days, while the QDs without
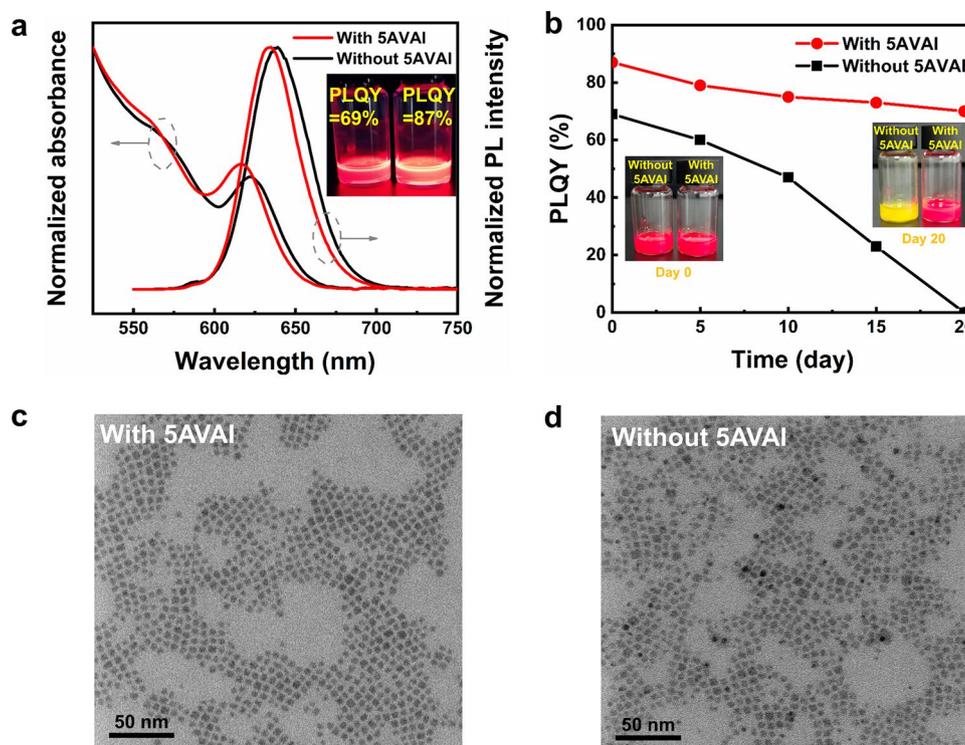
Fig. 2 **a** The UV–vis absorption and fluorescence spectra of CsPbI$_3$ QDs with and without 5AVAI were purified twice. The inset images show the photo of QDs (left: without 5AVAI; right: with 5AVAI) under ultraviolet (365 nm) and the corresponding PLQY value. **b** Stability of CsPbI$_3$ QD with and without 5AVAI under ambient conditions (temperature of 25 ± 5 °C and humidity of $50\pm10\%$), the inset images show the photos of two kinds of QDs after different storage days. TEM images of CsPbI$_3$ QDs **c** with and **d** without 5AVAI

5AVAI treatment decomposed after 20 days. These results show that 5AVAI ligands exchange the dynamical OA and OAm ligands on the QDs surface, which effectively passivate the surface defects of QDs and improve the stability of QDs. The effect of 5AVAI on the morphology of QDs was characterized by a TEM. Figure 2c, d shows the TEM images of CsPbI$_3$ QDs with and without 5AVAI, the 5AVAI-treated QDs maintain cubic shape and good monodispersity. In addition, compared with QDs without 5AVAI treatment (5.88 ± 1.16 nm), 5AVAI treatment has a smaller size (5.29 ± 0.76 nm) and a more uniform size distribution (the particle size distribution of QDs is shown in Fig. S3).

3.2 Interaction Between 5AVAI and CsPbI$_3$ QDs

To determine the interaction between QDs and 5AVAI ligands, the ligands on the surface of QDs were characterized. As shown in Fig. 3a, the signal peak at 1639 cm^{-1} represents the N–H bending vibration of the amine functional group [30],

and the peak at 1571 cm^{-1} is due to the asymmetric stretching vibration peak of carboxylate (COO$^-$) [31], which indicates that there are OA, OAm or 5AVAI ligands on QDs surface. After 5AVAI ligand treatment, the peak of the C–N stretching vibration signal at 907 cm^{-1} is enhanced [32, 33], indicating that the ligand containing amino functional groups on the QDs surface was increased due to the combination of 5AVAI ligand and QDs. In addition, the high-resolution XPS spectrum (Fig. S4) shows that the binding energy of Pb 4f in CsPbI$_3$ QDs treated with 5AVAI is significantly increased compared with the QDs without 5AVAI treatment. This shows that 5AVAI has a strong interaction with uncoordinated lead atoms on the surface of QDs, which makes the chemical environment of QDs change significantly. TGA showed that the weight of CsPbI$_3$ QDs with 5AVAI decreased by 32% at 500 °C, while the weight of CsPbI$_3$ QDs without 5AVAI decreased by 34%, indicating the decrease of long-chain ligands (Fig. 3b). XRD patterns (Fig. 3c) confirmed that the crystal structure of QDs did not change after treatment with 5AVAI ligands, all were
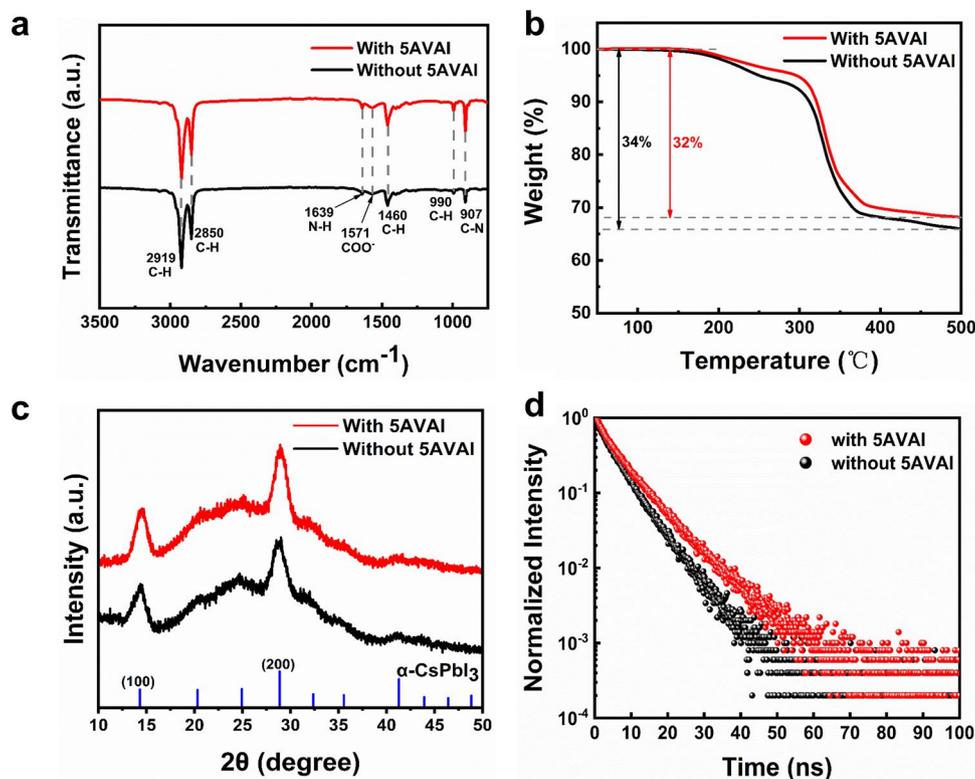
Fig. 3 **a** FTIR spectra of CsPbI$_3$ QDs with and without 5AVAI. **b** TGA of CsPbI$_3$ QDs with and without 5AVAI. **c** XRD spectra of CsPbI$_3$ QDs films with and without 5AVAI. **d** Time-resolved photoluminescence (TRPL) decay of CsPbI$_3$ QDs films with and without 5AVAI

the same cubic crystal structure. Time-resolved PL decay spectrum (Fig. 3d) shows that the average fluorescence lifetimes of CsPbI$_3$ QDs with and without 5VAI are 7.1 and 5.5 ns, respectively, which proves that the defects of CsPbI$_3$ QDs can be effectively reduced by 5VAI ligand treatment, leading to enhanced radiation recombination. AFM was used to characterize the surface morphology of CsPbI$_3$ QDs films with and without 5AVAI treatment (Fig. S5). The root mean square (RMS) roughness of CsPbI$_3$ QDs film with 5AVAI is 3.25 nm, while that of CsPbI$_3$ QDs film without 5AVAI is 5.73 nm. This is attributed to the exchange of some long-chain OA and OAm ligands between 5AVAI ligands, and the closer accumulation of QDs reduces the surface roughness of the films. This ensures good contact between the CsPbI$_3$ QDs layer and the hole transport layer.

3.3 Device Performance

QLEDs devices using CsPbI$_3$ QDs films with and without 5AVAI treatment as emitting layers were fabricated.

Figure 4a illustrates the QLEDs device structure which is composed of ITO/PEDOT:PSS/PTAA/CsPbI$_3$ QDs/ TmPyPB/PO-T2T/LiF/Al, where ITO is the anode and PEDOT:PSS is the hole injection layer, PTAA is the hole transport/electron barrier layer, TmPyPB/PO-T2T is the electron transport layer, and LiF/Al is the cathode. The thin TmPyPB electron transport layer inhibits the quenching of excitons produced in the QDs emission layer by the POT2T layer (Fig. S6). The cross-sectional TEM image of the device is shown in Fig. S7. According to the Tauc curve (Fig. S8) and ultraviolet photoelectron spectroscopy (UPS) diagram (Fig. S9) of the thin film of CsPbI$_3$ QDs with and without 5AVAI treatment, the device energy level diagrams of all functional layers are obtained (Fig. S10). Figure 4b shows the normalized electroluminescence spectra of CsPbI$_3$ QDs films with and without 5AVAI ligand treatment, with electroluminescence peaks at 645 and 651 nm, respectively. The corresponding CIE 1931 color coordinate of CsPbI$_3$ QDs treated by 5AVAI ligand is (0.710, 0.289) (Fig. 4c). In the range of applied bias voltage (3.1–5.8 V), the EL spectrum of QLEDs based on CsPbI$_3$ QDs treated with 5VAI showed
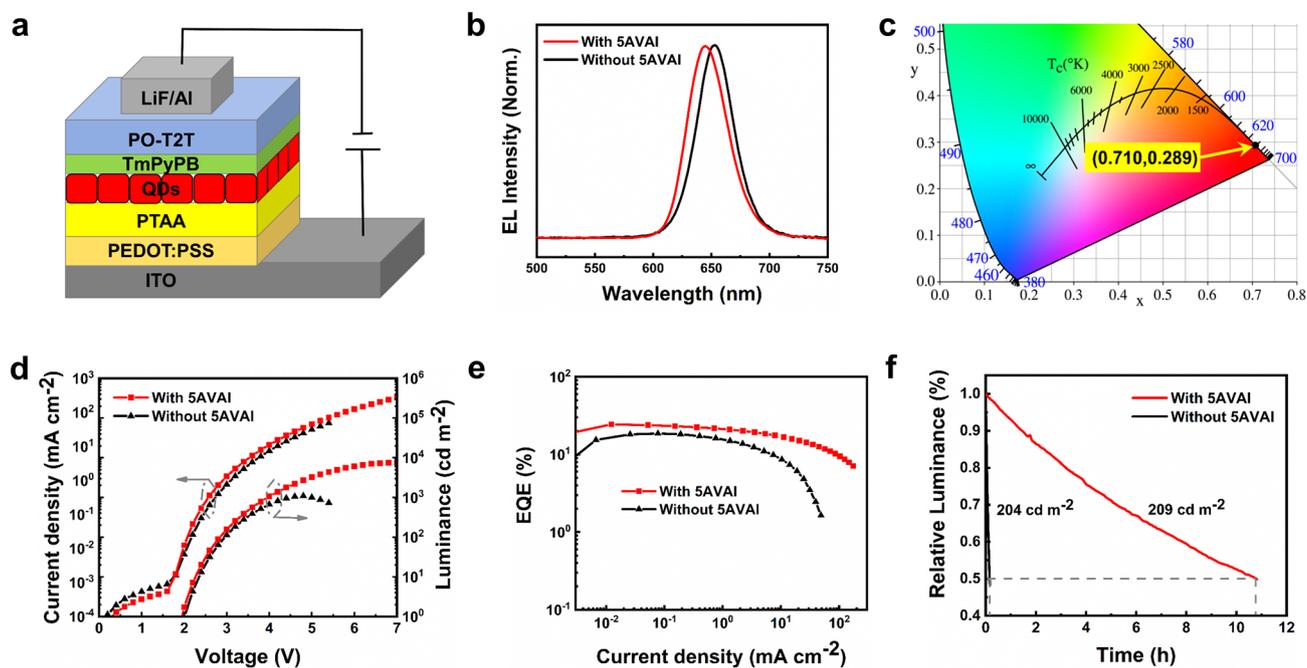
Fig. 4 a QLEDs device structure diagram. **b** Normalized electroluminescence spectra of CsPbI$_3$ QDs devices with and without 5AVAI treatment. **c** CIE coordinates correspond to the electroluminescence spectra of devices based on 5AVAI-treated CsPbI$_3$ QDs. QLEDs operating characteristics based on CsPbI$_3$ QDs with and without 5AVAI: **d** current density and luminance-voltage curve; **e** EQE-current density curve. **f** QLEDs stability based on CsPbI$_3$ QDs with and without 5AVAI treatment

excellent color stability, while the EL spectrum of devices without 5VAI treatment shifted slightly at high voltage (Fig. S11).

Figure 4d shows the current density-voltage-brightness (*J-V-L*) characteristics of champion QLEDs based on these two kinds of CsPbI$_3$ QDs. The high-quality thin film of QDs treated by 5AVAI makes the device have lower leakage current density. QLEDs based on 5AVAI treatment show significantly higher current density and brightness, and the maximum luminance is increased from 1090 to 7494 cd m^{-2}. This is attributed to the exchange of short-chain 5AVAI ligands between long-chain OA and OAm ligands, which increases the charge transfer between CsPbI$_3$ QDs and improves the performance of the device. The measurement of space-charge-restricted-current (SCLC) (Fig. S12) shows that the charge mobility of QDs films after 5AVAI treatment is increased. The peak EQE of QLEDs based on CsPbI$_3$ QD with and without 5AVAI is 24.45% and 18.63% (Fig. 4e), respectively, and the devices treated with 5AVAI show lower efficiency rolling at high current density. The improvement in device performance is attributed to that 5AVAI passivates the surface defects of QDs and inhibits non-radiative

recombination. In addition, the short-chain 5AVAI ligand improves the conductivity of QDs thin films and balances the carrier transport. Figure S6 shows the EQE histogram of 20 devices, which shows good repeatability. Finally, we evaluate the operational stability of QLEDs (Fig. 4f). At the initial brightness of 209 cd m^{-2}, the T$_{50}$ (the time required to decay to 50% of its initial value) of the CsPbI$_3$ QDs device with 5AVAI treatment is about 10.79 h, and that of the QDs device without 5AVAI treatment is 0.15 h (the initial brightness is 204 cd m^{-2}). After 5AVAI ligand treatment, the T$_{50}$ of the device is improved by about 70 times, which improves the operation stability of the device. The performance of our LEDs devices represents the best performance of bright red (EL < 650 nm) PeLEDs (Table S1).

4 Conclusions

In summary, we have developed a proton-prompted ligand exchange strategy on the surface of CsPbI$_3$ QDs, and the effective ligand exchange significantly improved the performance of the device. In this strategy, HI provides proton-driven OA and OAm ligands desorption dynamically bound

to QDs surface and realized in-situ exchange with 5AVAI ligands. The treatment of 5AVAI ligands significantly improved the stability and optical properties of $CsPbI_3$ QDs. We used these stable 5AVAI-treated $CsPbI_3$ QDs to fabricate bright red QLED with narrow electroluminescence at 645 nm. Short-chain 5AVAI ligand treatment significantly increased the current density and brightness of the device, achieving a record EQE of 24.45% and the T_{50} of 10.7 h, an increase of about 70 times. Our work provides a new method for ligand exchange of small-size $CsPbI_3$ QDs, and it is also an effective way to improve the performance of perovskite QLEDs.

Author Contributions YL and CX conceived the study. YL synthesized perovskite quantum dot materials and tested their optical properties. MD fabricated the LEDs device and characterized the device performance. XZ assisted in the synthesis of perovskite quantum dot materials and participated in the analysis of experimental data. CX and LQ supervised the project and provided advice. We cherish the memory of LQ and thank him for his contribution to our article. All authors discussed the results and commented on the paper.

Declarations

References

1. P. Fu, Q. Shan, Y. Shang, J. Song, H. Zeng et al., Perovskite nanocrystals: synthesis, properties and applications. Sci. Bull. **62**(5), 369–380 (2017). https://doi.org/10.1016/j.scib.2017.01.006

2. J. Shamsi, A.S. Urban, M. Imran, L. De Trizio, L. Manna, Metal halide perovskite nanocrystals: synthesis, post-synthesis modifications, and their optical properties. Chem. Rev. **119**(5), 3296–3348 (2019). https://doi.org/10.1021/acs.chemrev.8b00644

3. X.-K. Liu, W. Xu, S. Bai, Y. Jin, J. Wang et al., Metal halide perovskites for light-emitting diodes. Nat. Mater. **20**, 10–21 (2021). https://doi.org/10.1038/s41563-020-0784-7

4. J.S. Kim, J.M. Heo, G.S. Park, S.J. Woo, C. Cho et al., Ultra-bright, efficient and stable perovskite light-emitting diodes. Nature **611**, 688–694 (2022). https://doi.org/10.1038/s41586-022-05304-w

5. Y.-K. Wang, K. Singh, J.-Y. Li, Y. Dong, X.-Q. Wang et al., In situ inorganic ligand replenishment enables bandgap stability in mixed-halide perovskite quantum dot solids. Adv. Mater. **34**(21), e2200854 (2022). https://doi.org/10.1002/adma.202200854

6. Y. Wang, C. Duan, X. Zhang, J. Sun, X. Ling et al., Electroluminescent solar cells based on $CsPbI_3$ perovskite quantum dots. Adv. Funct. Mater. **32**(6), 2108615 (2022). https://doi.org/10.1002/adfm.202108615

7. A. Swarnkar, A.R. Marshall, E.M. Sanehira, B.D. Chernomordik, D.T. Moore et al., Quantum dot-induced phase stabilization of α-$CsPbI_3$ perovskite for high-efficiency photovoltaics. Science **354**(6308), 92–95 (2016). https://doi.org/10.1126/science.aag2700

8. W. Zhou, F. Sui, G. Zhong, G. Cheng, M. Pan et al., Lattice dynamics and thermal stability of cubic-phase $CsPbI_3$ quantum dots. J. Phys. Chem. Lett. **9**(17), 4915–4920 (2018). https://doi.org/10.1021/acs.jpclett.8b02036

9. J.-S. Yao, J. Ge, K.-H. Wang, G. Zhang, B.-S. Zhu et al., Few-nanometer-sized α-$CsPbI_3$ quantum dots enabled by strontium substitution and iodide passivation for efficient red-light emitting diodes. J. Am. Chem. Soc. **141**(5), 2069–2079 (2019). https://doi.org/10.1021/jacs.8b11447

10. L. Martínez-Sarti, S.H. Jo, Y.H. Kim, M. Sessolo, F. Palazon et al., Low-dimensional iodide perovskite nanocrystals enable efficient red emission. Nanoscale **11**(27), 12793–12797 (2019). https://doi.org/10.1039/c9nr04520a

11. Y.-F. Lan, J.-S. Yao, J.-N. Yang, Y.-H. Song, X.-C. Ru et al., Spectrally stable and efficient pure red $CsPbI_3$ quantum dot light-emitting diodes enabled by sequential ligand post-treatment strategy. Nano Lett. **21**(20), 8756–8763 (2021). https://doi.org/10.1021/acs.nanolett.1c03011

12. S. ten Brinck, F. Zaccaria, I. Infante, Defects in lead halide perovskite nanocrystals: analogies and (many) differences with the bulk. ACS Energy Lett. **4**(11), 2739–2747 (2019). https://doi.org/10.1021/acsenergylett.9b01945

13. Y. Dong, Y.-K. Wang, F. Yuan, A. Johnston, Y. Liu et al., Bipolar-shell resurfacing for blue LEDs based on strongly confined perovskite quantum dots. Nat. Nanotechnol. **15**, 668–674 (2020). https://doi.org/10.1038/s41565-020-0714-5

14. J. Pan, L.N. Quan, Y. Zhao, W. Peng, B. Murali et al., Highly efficient perovskite-quantum-dot light-emitting diodes by surface engineering. Adv. Mater. **28**(39), 8718–8725 (2016). https://doi.org/10.1002/adma.201600784

15. G. Li, J. Huang, H. Zhu, Y. Li, J.-X. Tang et al., Surface ligand engineering for near-unity quantum yield inorganic halide perovskite QDs and high-performance QLEDs. Chem. Mater. **30**(17), 6099–6107 (2018). https://doi.org/10.1021/acs.chemmater.8b02544

16. Y.-K. Wang, F. Yuan, Y. Dong, J.-Y. Li, A. Johnston et al., All-inorganic quantum-dot LEDs based on a phase-stabilized α-$CsPbI_3$ perovskite. Angew. Chem. Int. Ed. **60**(29), 16164–16170 (2021). https://doi.org/10.1002/anie.202104812

17. H. Zhao, H. Chen, S. Bai, C. Kuang, X. Luo et al., High-brightness perovskite light-emitting diodes based on $FAPbBr_3$ nanocrystals with rationally designed aromatic ligands. ACS Energy Lett. **6**(7), 2395–2403 (2021). https://doi.org/10.1021/acsenergylett.1c00812

18. A. Pan, B. He, X. Fan, Z. Liu, J.J. Urban et al., Insight into the ligand-mediated synthesis of colloidal $CsPbBr_3$ perovskite nanocrystals: the role of organic acid, base, and cesium precursors. ACS Nano **10**(8), 7943–7954 (2016). https://doi.org/10.1021/acsnano.6b03863

19. J. Shamsi, Z. Dang, P. Bianchini, C. Canale, F. Di Stasio et al., Colloidal synthesis of quantum confined single crystal $CsPbBr_3$ nanosheets with lateral size control up to the micrometer range. J. Am. Chem. Soc. **138**(23), 7240–7243 (2016). https://doi.org/10.1021/jacs.6b03166

20. F. Haydous, J.M. Gardner, U.B. Cappel, The impact of ligands on the synthesis and application of metal halide perovskite nanocrystals. J. Mater. Chem. A **9**(41), 23419–23443 (2021). https://doi.org/10.1039/d1ta05242j

21. S. Cho, J. Kim, S.M. Jeong, M.J. Ko, J.-S. Lee et al., High-voltage and green-emitting perovskite quantum dot solar cells via solvent miscibility-induced solid-state ligand exchange. Chem. Mater. **32**(20), 8808–8818 (2020). https://doi.org/10.1021/acs.chemmater.0c02102

22. D. Jia, J. Chen, J. Qiu, H. Ma, M. Yu et al., Tailoring solvent-mediated ligand exchange for $CsPbI_3$ perovskite quantum dot solar cells with efficiency exceeding 16.5%. Joule **6**(7), 1632–1653 (2022). https://doi.org/10.1016/j.joule.2022.05.007

23. Y. Sun, H. Zhang, K. Zhu, W. Ye, L. She et al., Research on the influence of polar solvents on $CsPbBr_3$ perovskite QDs. RSC Adv. **11**(44), 27333–27337 (2021). https://doi.org/10.1039/d1ra04485k

24. D. Liu, Z. Shao, C. Li, S. Pang, Y. Yan et al., Structural properties and stability of inorganic $CsPbI_3$ perovskites. Small Struct. **2**(3), 2000089 (2021). https://doi.org/10.1002/sstr.202000089

25. S. Kajal, J. Kim, Y.S. Shin, A.N. Singh, C.W. Myung et al., Unfolding the influence of metal doping on properties of $CsPbI_3$ perovskite. Small Methods **4**(9), 2000296 (2020). https://doi.org/10.1002/smtd.202000296

26. S.R. Smock, Y. Chen, A.J. Rossini, R.L. Brutchey, The surface chemistry and structure of colloidal lead halide perovskite nanocrystals. Acc. Chem. Res. **54**(3), 707–718 (2021). https://doi.org/10.1021/acs.accounts.0c00741

27. F. Krieg, S.T. Ochsenbein, S. Yakunin, S. Ten Brinck, P. Aellen et al., Colloidal CsPbX3 (X = Cl, Br, I) nanocrystals 2.0: Zwitterionic capping ligands for improved durability and stability. ACS Energy Lett. **3**(3), 641–646 (2018). https://doi.org/10.1021/acsenergylett.8b00035

28. J. De Roo, M. Ibáñez, P. Geiregat, G. Nedelcu, W. Walravens et al., Highly dynamic ligand binding and light absorption coefficient of cesium lead bromide perovskite nanocrystals. ACS Nano **10**(2), 2071–2081 (2016). https://doi.org/10.1021/acsnano.5b06295

29. Y. Dong, T. Qiao, D. Kim, D. Parobek, D. Rossi et al., Precise control of quantum confinement in cesium lead halide perovskite quantum dots via thermodynamic equilibrium. Nano Lett. **18**(6), 3716–3722 (2018). https://doi.org/10.1021/acs.nanolett.8b00861

30. S. Akhil, V.G.V. Dutt, N. Mishra, Completely amine-free open-atmospheric synthesis of high-quality cesium lead bromide ($CsPbBr_3$) perovskite nanocrystals. Chem. Eur. J. **26**(71), 17195–17202 (2020). https://doi.org/10.1002/chem.202003891

31. L.C. Cass, M. Malicki, E.A. Weiss, The chemical environments of oleate species within samples of oleate-coated PbS quantum dots. Anal. Chem. **85**(14), 6974–6979 (2013). https://doi.org/10.1021/ac401623a

32. L. Wu, Q. Zhong, D. Yang, M. Chen, H. Hu et al., Improving the stability and size tunability of cesium lead halide perovskite nanocrystals using trioctylphosphine oxide as the capping ligand. Langmuir **33**(44), 12689–12696 (2017). https://doi.org/10.1021/acs.langmuir.7b02963

33. W. Zheng, Z. Li, C. Zhang, B. Wang, Q. Zhang et al., Stabilizing perovskite nanocrystals by controlling protective surface ligands density. Nano Res. **12**, 1461–1465 (2019). https://doi.org/10.1007/s12274-019-2407-7